Appl Phys A (2012) 108:685–691
DOI 10.1007/s00339-012-6951-1

Applied Physics A
Materials Science & Processing

Laser sintering of silver nanoparticle thin films: microstructure and optical properties

P. Peng · A. Hu · Y. Zhou

Received: 4 October 2011 / Accepted: 13 April 2012 / Published online: 5 May 2012

Abstract We present a method for the sintering of silver (Ag) nanoparticle thin films by millisecond pulsed laser irradiation. The microstructure of sintered thin films and sintering behaviors of nanoparticles were systematically investigated in this paper. Absorption spectra of sintered thin films showed blue-shifted surface plasmon resonances (SPR) from 500 nm to 480 nm and red-shifted from 480 nm to 550 nm when laser power was varied from 100 W to 140 W and from 140 W to 200 W, respectively. This indicates a new technique to control light absorption through joining nanoparticles with laser sintering. According to theoretical calculations based on a heat diffusion model, the melting temperature of these Ag nanoparticles was estimated to be 440 °C during laser irradiation.

1 Introduction

For nanodevices and nanosystems, it is necessary to join nanoscale building blocks together to achieve complex functions [1, 2], such as joining metallic nanomaterials for potential applications in optical devices and flexible electronics because of their unique optical, electrical properties [3, 4]. For example, the surface plasmon resonance (SPR) of noble metal nanostructures and its strong absorption of light [5] have been the focus of numerous studies due to their practical applications in the fabrication of optical devices such as optical sensors, surface-enhanced Raman scattering probes or light filters [6–8]. The SPR position [9], shape [10] and spectral width [11] can be controlled through altering the excitation of oscillations in an electromagnetic field with changing particle size, shape, and the neck size of welded metallic nanoparticles (MNPs) [12–17]. Another example is the joining of noble MNPs by sintering in inkjet printing for flexible electronics [18–20], a well-known technique in which the deposition and patterning are simultaneously accomplished by printing a solution of the active materials (e.g., MNPs or conductive polymers). MNP ink typically consists of gold or silver nanoparticles (Ag NPs) encapsulated with a thin protective shell and dispersed in a liquid solvent [21, 22]. Thermal heating, e.g., by ovens and furnaces, is usually used for sintering of MNPs. For example, low temperature oven sintering of Ag NPs and their bonding to copper wires and substrates for applications in flexible electronics have been reported by Hu et al. [23] and Alarifi et al. [24]. The typical sintering temperature ranges from 100–300 °C which is lower than the melting point of the corresponding bulk materials, due to the size effect of nanoparticles [25].

However, thermal sintering possesses numerous drawbacks, e.g., time-consuming, low heating rate and not area-specific [26]. As alternatives, more precise sintering techniques are developed to accurately tailor the nanostructure of the materials, such as applying voltage [26], microwave [27, 28], and laser beam [29–35]. Sanchez-Valencia et al. [36] studied the effect of laser power on the structure and optical dichroism of self-organized metal nanostructures by nanosecond laser treatment of Ag nanostripes supported on SiO_2 nanocolumns. Laser sintered TiO_2 film have been study for dye-sensitized solar cells [37, 38]. However, very

P. Peng (✉) · A. Hu · Y. Zhou
Centre for Advanced Materials Joining, Department of Mechanical and Mechatronics Engineering, University of Waterloo, 200 University Avenue West, Waterloo, ON, N2L 3G1, Canada
e-mail: p5peng@uwaterloo.ca
Fax: +1-519-8886197

P. Peng · Y. Zhou
Waterloo Institute for Nanotechnology, University of Waterloo, 200 University Avenue West, Waterloo, ON, N2L 3G1, Canada

few reports have focused on the effect of laser irradiation on the structure and optical properties of self-organized Ag nanoparticle thin films. In this paper, we have studied the microstructure and optical properties of sintered Ag NP thin films as a function of the millisecond laser power.

2 Experimental details

Silver nitrate ($AgNO_3$, Alfa Aesar), polyvinylpyrrolidone or PVP ($(C_6H_9NO)_n$, K25, M.W. = 24000, Alfa Aesar), sodium citrate ($C_6H_5O_7Na_3{\cdot}2H_2O$, Alfa Aesar), and ascorbic acid or VC ($C_6H_8O_6$, Alfa Aesar) were used without further purification. In a typical synthesis, the Ag NP solution was prepared by adding 12 ml sodium citrate aqueous solution (0.2 M) to 200 ml deionized water with vigorous stirring, followed by adding 2 ml PVP aqueous solution (20 mM), 2 ml $[Ag(NH_3)_2]^+$ aqueous solution (0.12 M), and 0.4 ml Ag seed (1 mM, size is about 5 nm). Then 10 ml VC aqueous solution (10 mM) was dropwise added into the mixture for 30 minutes with stirring. Microscopy glass slides and silica wafers were all washed using acetone and deionized water then dried at 100 °C in oven, then immersed into Ag NP solution for at least 48 hours. The solution-deposited glass slides were used to characterize the optical properties and Si wafers were employed for investigations of microstructure and sintering behaviors.

Thin films on glass and Si wafer substrates were irradiated by a Nd:YAG-pulsed laser (Miyachi LW-50A, wavelength = 1064 nm, pulse width = 1 ms, repetition rate = 200 Hz, maximum average power = 5 kW, and focused beam size = 0.6 mm) for 1 ms time interval at different laser powers without using a photoresist layer. The morphology of the as-synthesized Ag NPs, deposited and sintered Ag NP thin films on glass and Si wafer substrates were characterized by scanning probe microscopy (SPM, Vecco 3100) and scanning electron microscopy (SEM, LEO 1530), respectively. Absorbance spectra of laser processed thin films (within the laser continually scanned 1 cm × 1 cm area) were measured with UV-vis-NIR spectroscopy (Shimadzu, UV-2500).

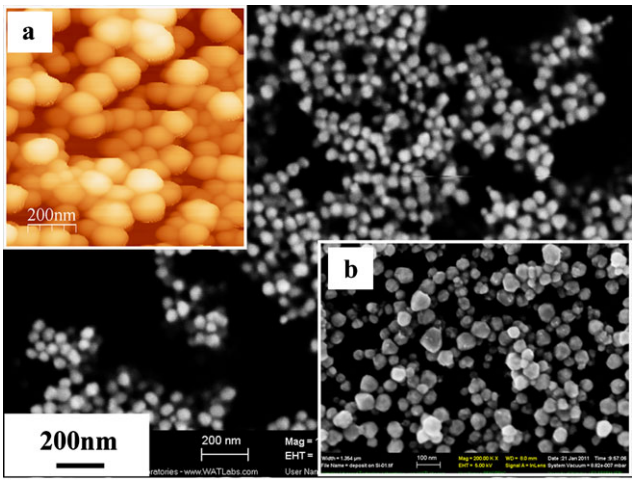

Fig. 1 Microstructures of Ag NPs in solution (average size 50 nm in diameter), inserted image (**a**) AFM image of thin film on glass substrate and (**b**) SEM image of thin film deposited on Si wafer

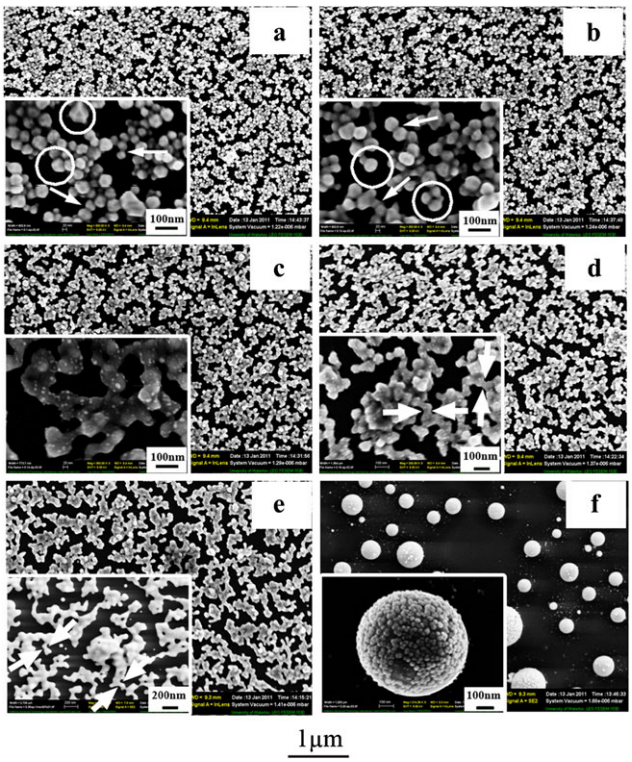

Fig. 2 SEM images of Ag NP thin films on Si substrate irradiated at different laser powers, (**a**) to (**f**) denoting irradiation using 100 W, 120 W, 140 W, 160 W, 180 W, and 200 W laser power, respectively, with *insets* showing corresponding images at high magnification

3 Results and discussion

3.1 Microstructure and sintering behaviors

Figure 1 shows Ag NPs in solution with an average diameter of 50 nm, and the microstructure of Ag NP thin films on glass and Si wafer substrates (insert images (a) and (b), respectively). It was found that Ag NPs aggregated together by self-organization in clusters on substrates and formed thin films. Since the microstructures of thin films (pristine and processed) on glass and Si substrates were found to be similar, all the microstructure discussions are all based on Si substrate below.

Figure 2 shows the microstructure of Ag NP thin films within the focused laser beam after irradiation with different laser powers. It can be seen that the degree of aggregation

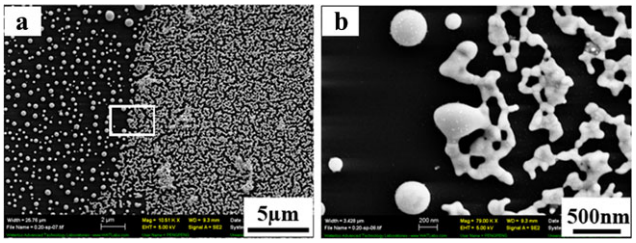

Fig. 3 (**a**) Transition from solid-state sintering of Ag NPs to the melting and coalescence of molten Ag NPs to form large independent Ag NP spheres, using 200 W laser power, at the boundary region of focused laser beam and (**b**) high magnification image of highlighted area in (**a**)

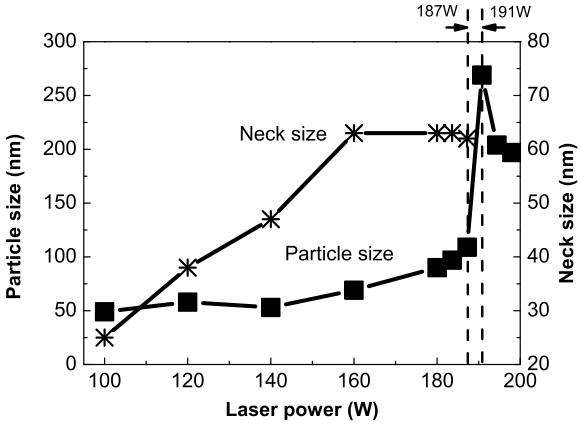

Fig. 4 The statistical Ag NP diameter and neck size as functions of laser power. Highlighted zone corresponded to the solid-liquid transition between 187 W to 191 W

increased with increased laser power. Ag NPs displayed a polyhedral shape at the power of 100 W (insert to Fig. 2a, highlighted in the circles). Usually, the vertex and edge of polyhedron shaped Ag NPs are facile to change under heating due to their high surface energy. With further increase in laser power, the polyhedral Ag NPs changed to relatively smooth spherical shapes (Fig. 2b inserted image, highlighted in the circles). Then the Ag NPs started to form bent chains and networks by joining the adjacent nanoparticles together. The necks formed and grew (as highlighted by the arrows in Fig. 2a & b) while the particle size remained unchanged at this stage. As the laser power rose further, it was clear to see that while the necks grew further and the particles started to become bigger than in the previous stage from the inserted high magnification images in Fig. 2(c–e). With the neck size increasing as highlighted by the pairs of arrows in Fig. 2d and e, the curvature of neck area decreased. However, Fig. 2f presents the very distinct morphology (independent spheres with diameters of few hundred nanometers) which corresponds to the solid-liquid transition [39, 40], under 200 W laser irradiation. A solidification pattern was clearly shown on the surface of the spheres as the high magnification image shown in Fig. 2f. These large spheres were formed by coalescence of molten Ag NPs because of surface tension. This general trend in the formation and growth of the necks, the growth of the particles, and the transition to the melted and coalesced Ag NPs could be clearly observed at the boundary region of the irradiated area when laser power of 200 W was used as shown in Fig. 3. The center with resolidified NPs is within the focused laser beam.

The changes in the neck and particle size within the focused laser beam were plotted as shown in Fig. 4 in which all neck and particle sizes were obtained by statically measuring no less than 10 particles/necks and the mean sizes were used (the maximum error is ± 8.2 %). It could be seen that the neck size grew linearly when the laser irradiation power was from 100 W to 160 W. The small change in neck size from 160 W to 187 W was mainly due to the decreasing driving force caused by the decreased curvature of neck area as neck size grew. The particle size remained stable at low laser powers (<140 W) and slowly grew as the laser power increased from 140 W to 187 W. The particle size grew rapidly after 187 W as shown in the highlighted zone in Fig. 4, corresponded to the melting of Ag NP clusters. When the laser energy was larger than 191 W, melting and evaporation contributed to the decrease in particle size with further rise in laser power. Due to the fast heating rate during laser sintering, the sequence was different compared to that of thermal sintering. The initial neck/particle growth during thermal heating was very fast, exponentially, then slowed down according to experimental and simulative results [23].

3.2 Light absorption properties

The absorption spectra of Ag NP solution and thin film without laser irradiation are shown in Fig. 5a. Ag NP solution displays a characteristic peak of Ag NPs centered at 430 nm, which is in accordance with the reported absorption peak of Ag NP aquatic solutions [41–43]. Two broad SPR bands are shown in the spectra of the Ag NP thin film. The first band, corresponding to the characteristic absorption peak of the Ag NPs, shifted to near 400 nm due to the smaller distances between the nanoparticles than those in solution and the change of medium. The smaller distances led to the enhanced quadrupolar oscillation of Ag NPs [44], which would cause the shift to lower wavelength. Decreasing of the dielectric constant of the surrounding medium, from water to air, was found to reduce the absorption wavelength in studies of gold nanorods [45] and periodic Ag NPs [46, 47]. Another broad SPR band near 750 nm (indicated as the 2nd peak in Fig. 5a) corresponds to longitudinal surface plasmon absorption [48, 49] formed from the aggregation of Ag NPs in the thin film and the sharp corners of polyhedron shaped Ag NPs [50]. The disappearance of the longitudinal surface plasmon absorption spectrum in Fig. 5b might be attributed to weakened longitudinal oscillations of electrons [51, 52]

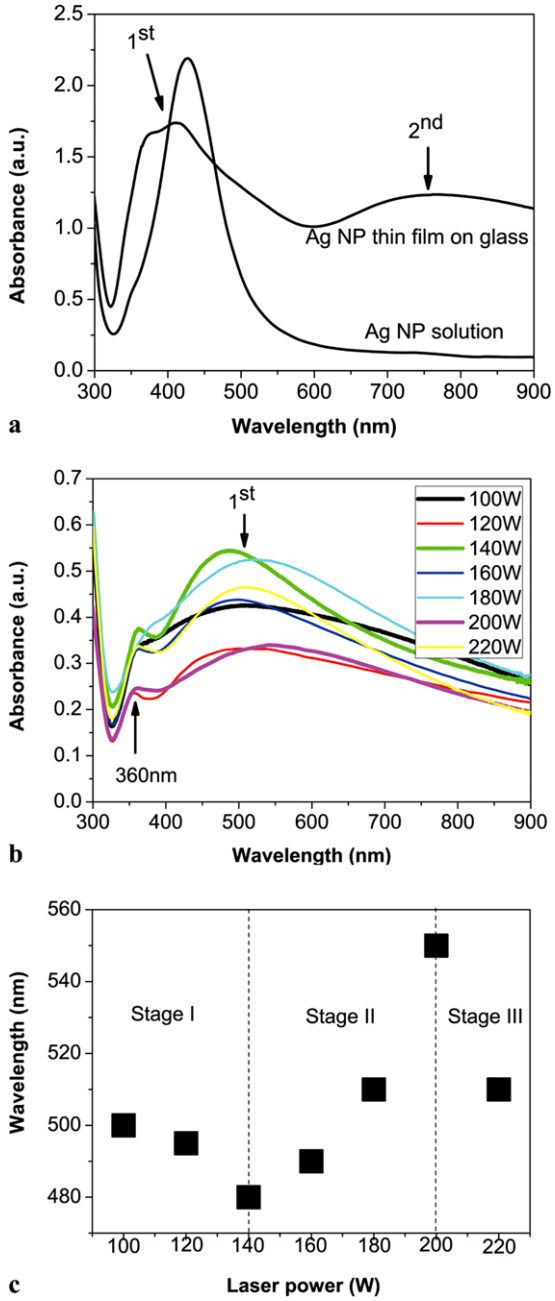

Fig. 5 Absorption spectra of (**a**) Ag NP solution and as-deposited Ag NP thin film without laser irradiation and (**b**) sintered Ag NP thin films under different laser powers. (**c**) The wavelength of nominal absorption peak of Ag NP thin films measured after irradiation at different laser powers (three stages: organic shell decomposition; neck and particles growth; melting and evaporation)

caused by reduced Ag NP aggregation and smooth curvature of Ag NPs after laser irradiation. The first SPR of Ag NP thin film was shifted and broader after laser irradiation as shown in Fig. 5b, which will be discussed in detail later. There were small peaks near 360 nm, which is attributed to the electronic interband transitions related absorption of silver [53–55]. This peak was not significant in Fig. 5a because of the much stronger intensity of other SPR peaks.

Further details of the change in characteristic peak (indicated as the 1st peak in Fig. 5b) as a function of laser power are plotted in Fig. 5c. The shifts of the nominal peak could be separated into three stages: (I) shifts from 500 nm to lower wavelength 480 nm (blueshift) at low laser powers, (II) recovering to 550 nm (redshift) at intermediate laser powers and (III) the dramatic decrease in wavelength when the laser power was more than 200 W.

The wavelength of a SPR peak is dependent on the shape and size of MNPs [56] and their distance, such as aggregated or joined MNPs [12, 44]. When Ag NP films are irradiated using different laser powers, the distance and shape of Ag NPs can be changed. Here, blue-shifted SPR of Ag films irradiated at low laser powers as illustrated in Fig. 5c stage 1 was attributed to decomposition of organic shells and the improvement in the symmetry of the nanoparticle shapes [57–59], from polyhedral to spherical shape. The spherical nanoparticles gained more symmetry in comparison with polyhedron shaped Ag NPs. Since the particle size did not change much, the improved symmetry of Ag NPs caused intensive excitation of high-order modes of quadrupole and octopole oscillations and contributed to the blue-shift. With the laser power further increasing, necks between joined Ag NPs and particle size grew during stage 2 (Fig. 5c stage 2). The enhanced interparticle coupling between joined Ag NPs caused by the neck size growth, means decreasing interparticle spacing, contributed to distorted intraparticle charge distribution [44] in which strong localized charges could occur near the neck area and cause strong attractive interaction across the neck. The intensive interaction (or lower-order mode of dipole oscillations) reduced the intraparticle restoring forces of distorted charges in joined Ag NPs and lowered the resonant energies [44, 60, 61] that generated the red-shift of absorption peak. However, the SPR peak suddenly decreased as the laser power keeping increasing to 220 W, which was due to the disappearance of necks, decreased particle size and the weakened SPR of the Ag NPs [12, 55]. Unlike the dichroism of nanosecond laser treated Ag nanostripes [36], this tunable light absorption of sintered Ag NP thin films by millisecond pulsed laser irradiation provides potential applications for optical devices, such as optical sensors.

4 Laser heating temperature

In order to further investigate the laser's effects and evaluate the temperature during laser irradiation, a heat diffusion model [62] is adopted in this section.

It is assumed that the Ag NP thin film has a very uniform thickness and that the laser beam is uniformly distributed in

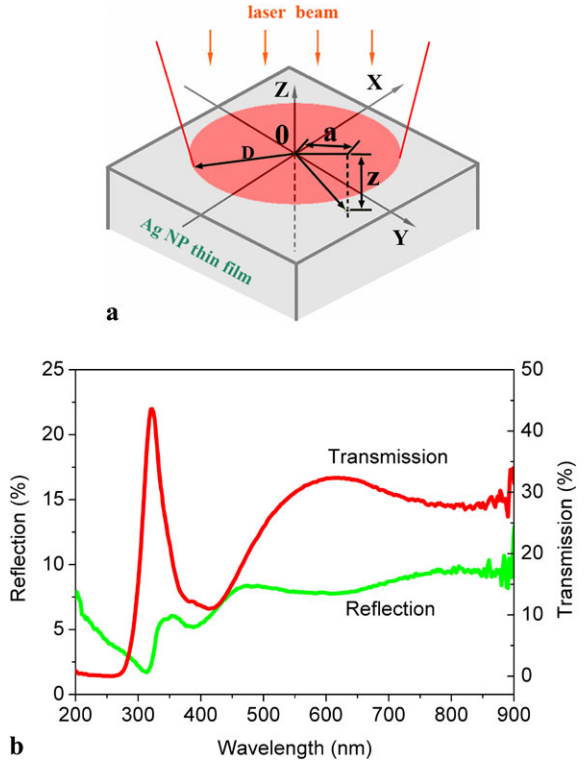

Fig. 6 (**a**) Schematic of the heat diffusion model for thin film; (**b**) The reflection and transmission properties of Ag NP thin film without laser irradiation

a circle of radius D. The absorptance α and specific heat capacity C of Ag NP thin film are constants. Employing the cylindrical coordinates in Fig. 6a, the temperature increase can be expressed as follows [62]:

$$\Delta T(a,Z,t) = \frac{\alpha P_0}{2\pi DK}\int_0^\infty \frac{d\lambda}{\lambda} J_0(\lambda a) J_1(\lambda D) \times \left\{ e^{-\lambda Z}\mathrm{erfc}\left[\frac{Z}{2(\kappa t)^{1/2}} - \lambda(\kappa t)^{1/2}\right] - e^{-\lambda Z}\mathrm{erfc}\left[\frac{Z}{2(\kappa t)^{1/2}} + \lambda(\kappa t)^{1/2}\right]\right\} \quad (1)$$

where K and κ denote thermal conductivity and thermal diffusivity. J_0 and J_1 are Bessel functions of the first kind. At $a = 0$, the equation yields the temperature of the center of the laser beam spot ($a = 0$ in Fig. 6a), and on axis $Z = 0$, the above equation can be simplified as follows:

$$\Delta T = \frac{2\alpha P_0}{\pi^{3/2} D^2 K}(\kappa t_\mathrm{p})^{1/2} \quad (2)$$

If laser beam radius D, the thermal conductivity K and thermal diffusivity κ are all constants, the temperature increase will be proportional to both laser power P_0 and the square root of laser pulse duration time t_p. In this study, the laser pulse duration time $t_\mathrm{p} = 1$ ms, beam radius $D = 0.03$ cm, the thermal diffusivity of Ag $\kappa = 1.74$ cm^2/s (at 300 K) and

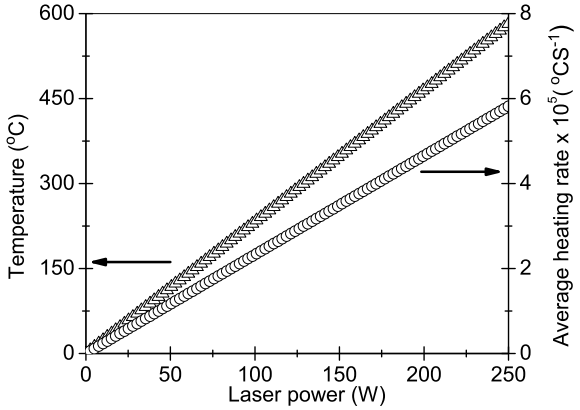

Fig. 7 Laser heating temperature and average heating rate as functions of laser power at the absorption coefficient α of 60 %

thermal conductivity $K = 4.29$ W cm^{-1} K^{-1} [63–65]. Using those constants, the temperature increase as a function of laser power can be rewritten as

$$\Delta T = 3.88 \times \alpha P_0 \quad (3)$$

where P_0 is in Watt and ΔT is in Celsius degree.

Reflection always exists in thin films. For smooth Ag thick films, the reflection coefficient R is usually around 98 % [66, 67]. However, in our case the surface of solution-deposited Ag NP thin films is very rough as observed in Fig. 1, the value of reflection for Ag NP thin film can be affected by the nanoparticle size and roughness [68, 69]. Nakashima's experimental and theoretical results at 1064 nm wavelength show that the reflection coefficient R is about 32 % [70]. According to the trends of reflection and transmission of Ag NP thin film in current measurement from 200 nm to 900 nm shown in Fig. 6b, we may estimate the reflection and transmission around 10 % and 30 %, respectively, at wavelength of 1064 nm (the measurement limit of our device is 900 nm). The absorptance α is thus about 60 %. The temperature and average heating rate ($\Delta T/t_\mathrm{p}$) as functions of laser power according to Eq. (3) can be plotted as shown in Fig. 7. The average heating rate of laser irradiation is very high at about 4×10^5 °C/s compared with conventional thermal sintering methods, e.g., ovens, hotplates, and furnaces typically at 2 °C/s.

The laser power of 187 W–191 W, which could cause melting according to the above optical property and microstructure analysis in the preceding section, corresponds to 435 °C–445 °C in Eq. (3) at $\alpha = 60$ %. It is long known that the melting point of Ag NPs is lower than that of bulk Ag materials [71–74]. For example, Yeshchenko [75] reported the melting temperature of 30 nm Ag NPs is about 350 °C. Hence, the calculated temperature can explain the variations of the spectral position and morphology of laser sintered Ag NP thin films when irradiated by 180 W to 200 W pulsed laser.

5 Conclusions

Millisecond pulsed laser irradiation was effectively used to precisely control the light absorption of Ag NP thin films deposited on glass substrates. A tunable light absorption behavior of Ag NP thin films was achieved by changing the shape and particle sizes of Ag NPs and also the neck size in joined Ag NPs via different laser powers. The results indicate potential applications for making light filters or optical sensors. The laser sintering behavior shows that the neck size grew linearly with laser power. According to the theoretical calculation using the heat diffusion model, the melting temperature of Ag NP at 50 nm in diameter is around 440 °C.

Acknowledgements This work was supported financially by the Canada Research Chairs (CRC) program, National Science and Engineering Research Council (NSERC) of Canada discovery grant and the State Scholarship Fund of China (No. 2010640009). The authors would like to acknowledge the comments and suggestions of Professor Scott Lawson and Dr. Xiaogang Li from the Centre for Advanced Materials Joining at the University of Waterloo.

References

1. Y. Zhou, *Microjoining and Nanojoining* (Woodhead, Cambridge, 2008)
2. Y. Zhou, A. Hu, Open Surf. Sci. J. **3**, 32 (2011)
3. J. Du, B. Han, Z. Liu, Y. Liu, Cryst. Growth Des. **7**, 900 (2007)
4. T. Teranishi, M. Hosoe, T. Tanaka, M. Miyake, J. Phys. Chem. B **103**, 3818 (1999)
5. W.A. Murray, E.L. Barnes, Adv. Mater. **19**, 3771 (2007)
6. J. Toudert, H. Fernandez, D. Babonneau, S. Camelio, T. Girardeau, J. Solis, Nanotechnology **20**, 475705 (2009)
7. H. Liang, Z. Li, W. Wang, Y. Wu, H. Xu, Adv. Mater. **21**, 4614 (2009)
8. A. Hu, W.W. Duley, Chem. Phys. Lett. **450**, 375 (2008)
9. J. Gonzalo, R. Serna, J. Solis, D. Babonneau, C.N. Afonso, J. Phys., Condens. Matter **15**, 3001 (2003)
10. J.S. Biteen, L.A. Sweatlock, H. Mertens, N.S. Lewis, A. Polman, H.A. Atwater, J. Phys. Chem. C **111**, 13372 (2007)
11. H. Hövel, S. Fritz, A. Hilger, U. Kreibig, M. Vollmer, Phys. Rev. B, Condens. Matter Mater. Phys. **48**, 18178 (1993)
12. T. Zhang, X.Y. Zhang, X. Xue, X. Wu, C. Li, A. Hu, Open Surf. Sci. J. 3, 78 (2011)
13. J.P. Barnes, A.K. Petford-Long, R.C. Doole, R. Serna, J. Gonzalo, A. Suárez-Garcia, C.N. Afonso, D. Hole, Nanotechnology **13**, 465 (2002)
14. B. Palpant, B. Prevel, J. Lermé, E. Cottancin, M. Pellarin, M. Treilleux, A. Perez, J.L. Vialle, M. Broyer, Phys. Rev. B, Condens. Matter Mater. Phys. **57**, 1998 (1963)
15. F. Stietz, Appl. Phys. A **72**, 381 (2001)
16. J. Toudert, S. Camelio, D. Babonneau, M.F. Denanot, T. Girardeau, J.P. Espinós, P. Yubero, A.R. Gonzalez-Elipe, J. Appl. Phys. **98**, 114316 (2005)
17. L. Simonot, D. Babonneau, S. Camelio, D. Lantiat, P. Guérin, B. Lamongie, V. Antad, Thin Solid Films **518**, 2637 (2010)
18. H. Sirringhaus, T. Kawase, R.H. Friend, T. Shimoda, M. Inbasekaran, W. Wu, E.P. Woo, Science **290**, 2123 (2000)
19. B. Ridley, B. Nivi, J.M. Jacobson, Science **286**, 746 (1999)
20. D. Redinger, S. Molesa, S. Yin, R. Farschi, V. Subramanian, IEEE Trans. Electron Devices **51**, 2004 (1978)
21. D. Kim, J. Moon. Electrochem. Solid-State Lett. **8**, J30 (2005)
22. H.H. Lee, K.S. Chou, K.C. Huang, Nanotechnology **16**, 2436 (2005)
23. A. Hu, J. Guo, H. Alarifi, G. Patane, Y. Zhou, G. Compagnini, C. Xu, Appl. Phys. Lett. **97**, 153117 (2010)
24. H. Alarifi, A. Hu, M. Yavuz, Y. Zhou, J. Electron. Mater. **40**, 1394 (2011)
25. P. Buffat, J.P. Borel, Phys. Rev. A **13**, 2287 (1976)
26. M.L. Allen, M. Aronniemi, T. Mattila, A. Alastalo, K. Ojanperä, M. Suhonen, H. Seppä, Nanotechnology **19**, 175201 (2008)
27. J. Perelaer, B. J. deGans, U. S. Schubert. Adv. Mater. **18**, 2101 (2006)
28. S. Uchida, M. Tomiha, N. Masaki, A. Miyazawa, H. Takizawa, Sol. Energy Mater. Sol. Cells **81**, 135 (2004)
29. E. Haberstroh, W.M. Hoffmann, R. Poprawe, F. Sari, Microsyst. Technol. **12**, 632 (2006)
30. N.R. Bieri, J. Chung, S.E. Haferl, D. Poulikakos, C.P. Grigoropoulos, Appl. Phys. Lett. **82**, 3529 (2003)
31. J. Chung, S. Ko, N.R. Bieri, C.P. Grigoropoulos, D. Poulikakos, Appl. Phys. Lett. **84**, 801 (2004)
32. S. Ko, H. Pan, C.P. Grigoropoulos, C.K. Luscombe, J.M.J. Fréchet, D. Poulikakos, Nanotechnology **18**, 345202 (2007)
33. D. Alloyeau, C. Ricolleau, C. Langlois, Y.L. Bouar, A. Loiseau, Beilstein J. Nanotechnology **1**, 55 (2010)
34. Y. Cheng, R. Uang, Y. Wang, K. Chiou, T. Lee, Microelectron. Eng. **86**, 865 (2009)
35. H. Pan, N. Misra, S.H. Ko, C.P. Grigoropoulos, N. Miller, E.E. Haller, O. Dubon, Appl. Phys. A **94**, 111 (2009)
36. J.R. Sanchez-Valencia, J. Toudert, A. Borras, A. Barranco, R. Lahoz, G.F. de la Fuente, F. Frutos, A.R. Gonzalez-Elipe, Adv. Mater. **23**, 848 (2011)
37. T. Watson, I. Mabbett, H. Wang, L. Peter, D. Worsley, Prog. Photovolt. Res. Appl. **19**, 482 (2011)
38. G. Mincuzzi, L. Vesce, A. Reale, A.D. Carlo, T.M. Brown, Appl. Phys. Lett. **95**, 103312 (2009)
39. Y. Wen, Y. Zhang, J. Zheng, Z. Zhu, S. Sun, J. Phys. Chem. C **113**, 20611 (2009)
40. V.A. Mandelshtam, P.A. Frantsuzov, F. Calvo, J. Phys. Chem. A **110**, 5326 (2006)
41. L. Lu, A. Kobayashi, K. Tawa, Y. Ozaki, Chem. Mater. **18**, 4894 (2006)
42. Y. Badr, M.G. Abd El Wahed, M.A. Mahmoud, Appl. Surf. Sci. **253**, 2502 (2006)
43. D. Aherne, D.M. Ledwith, M. Gara, J.M. Kelly, Adv. Funct. Mater. **18**, 2008 (2005)
44. R. Chen, X. Liu, C. Chang, Phys. Rev. E **76**, 016609 (2007)
45. S. Link, M.B. Mohamed, M.A. EI-Sayed, J. Phys. Chem. B **103**, 3073 (1999)
46. T.R. Jensen, M.L. Duval, K.L. Kelly, A.A. Lazarides, G.C. Schatz, R.P. Van Duyne, J. Phys. Chem. B **103**, 9846 (1999)
47. M.D. Malinsky, K.L. Kelly, G.C. Schatz, R.P. Van Duyne, J. Phys. Chem. B **105**, 2343 (2001)
48. R.A. Ganeev, M. Babba, A.I. Ryasnyansky, M. Suzuki, H. Kuroda, Opt. Commun. **240**, 437 (2004)
49. M. Kyoung, M. Lee, Opt. Commun. **171**, 145 (1999)
50. S.K. Ghosh, T. Pal, Chem. Rev. **107**, 4797 (2007)
51. L.M. Liz-Marzán, Langmuir **22**, 32 (2006)
52. C.S. Ah, H.S. Han, K. Kim, D. Jang, J. Phys. Chem. B **104**, 8153 (2000)
53. G. Fuster, J.M. Tyler, N.E. Brener, J. Callaway, D. Bagayoko, Phys. Rev. B **42**, 7322 (1990)
54. Z.S. Pillai, P.V. Kamat, J. Phys. Chem. B **108**, 945 (2004)
55. P. Taneja, P. Ayyub, Phys. Rev. B **65**, 245412 (2002)
56. Y. Sun, Y. Xia, Science **298**, 2176 (2002)

57. K. Nakayama, K. Tanabe, H.A. Atwater, Appl. Phys. Lett. **93**, 121904 (2008)
58. C.F. Bohren, D.R. Huffman, *Absorption and Scattering of Light by Small Particles* (Wiley, New York, 1983)
59. J.S. Biteen, N.S. Lewis, H.A. Atwater, Appl. Phys. Lett. **88**, 131109 (2006)
60. J.P. Kottmann, O.J.F. Martin, Opt. Express **8**, 655 (2001)
61. J. Aizpurua, G.W. Bryant, L.J. Richter, F.J. Garcia de Abajo, B.K. Kelley, T. Mallouk, Phys. Rev. B **71**, 235420 (2005)
62. M. Bertolotti, *Physical Processes in Laser-Materials Interactions* (Plenum Press, New York, 1983)
63. J.R. Davis, *Metals Handbook*, 2nd edn. (ASM International, Materials Park, 1998)
64. M.M. Rathore, R.R. Kapuno, *Engineering Heat Transfer*, 2nd edn. (Jones & Bartlett Learning, Boston, 2010)
65. F. Hemberger, H.P. Ebert, J. Fricke, Int. J. Theor. Phys. **28**, 1509 (2007)
66. H.W. Edwards, R.P. Petersen, Phys. Rev. **50**, 871 (1936)
67. I.V. Antonets, L.N. Kotov, S.V. Nekipelov, E.N. Karpushov, Tech. Phys. **49**, 1496 (2004)
68. Q. Li, C.W. Kuo, Z. Yang, P. Chen, K.C. Chou, Phys. Chem. Chem. Phys. **11**, 3436 (2009)
69. Q. Zhou, Y. Liu, Y. He, Z. Zhang, Y. Zhao, Appl. Phys. Lett. **97**, 121902 (2010)
70. H. Nakashima, M. Yonekura, J. Appl. Phys. **84**, 6286 (1998)
71. M. Mirjalili, J. Vahdati-Khaki, J. Phys. Chem. Solids **69**, 2116 (2008)
72. C.L. Chen, J.G. Lee, K. Arakawa, H. Mori, Appl. Phys. Lett. **96**, 253104 (2010)
73. Q. Jiang, S. Zhang, M. Zhao, Mater. Chem. Phys. **82**, 225 (2003)
74. D. Xie, M.P. Wang, W.H. Qi, L.F. Cao, Mater. Chem. Phys. **96**, 418 (2006)
75. O.A. Yeshchenko, I.M. Dmitruk, A.A. Alexeenko, A.V. Kotko, Nanotechnology **21**, 045203 (2010)